Journal of Nuclear Materials 433 (2013) 167–173

Contents lists available at SciVerse ScienceDirect

Journal of Nuclear Materials

journal homepage: www.elsevier.com/locate/jnucmat

Effect of vacancy on the dissolution and diffusion properties of hydrogen and helium in molybdenum

Yu-Wei You [a], Xiang-Shan Kong [a], Xue-Bang Wu [a], Q.F. Fang [a], Jun-Ling Chen [b], G.-N. Luo [b], C.S. Liu [a,*]

[a] Key Laboratory of Materials Physics, Institute of Solid State Physics, Chinese Academy of Sciences, P.O. Box 1129, Hefei 230031, PR China
[b] Institute of Plasma Physics, Chinese Academy of Sciences, Hefei 230031, PR China

HIGHLIGHTS

- Both H and He are more favorable to occupy the tetrahedral interstitial sites nearby a vacancy (or helium-vacancy complex) rather than that far away from the vacancy or complex.
- The diatomic hydrogen–hydrogen and helium–helium prefer ⟨100⟩ and ⟨111⟩ dumbbell configurations in single vacancy, respectively.
- The diffusion-out barriers of hydrogen and helium from a vacancy and helium-vacancy complex are much larger than diffusion-in barriers, especially for helium.
- Interstitial helium can reduce the nearby vacancy formation energy more significantly than hydrogen.

ARTICLE INFO

Article history:
Received 14 February 2012
Accepted 24 September 2012
Available online 5 October 2012

ABSTRACT

We present first-principles study of the stability and diffusion properties of H and He in Mo. The results show that diatomic H–H and He–He prefer ⟨100⟩ and ⟨111⟩ dumbbell configurations in single vacancy, respectively. The occupation and migration of H and He nearby a vacancy (or He-vacancy complex) are very different from that in bulk: both H and He are more preferable to occupy the tetrahedral interstitial sites closer to the vacancy (or He-vacancy complex), and the diffusion barriers of H and He into the vacancy (or He-vacancy complex) are slightly reduced but the diffusion barriers out of the defect are severely increased, especially for He. Besides, the presence of single He at tetrahedral interstitial site reduces the energy required for its nearby vacancy formation more considerably than that of H (the produced vacancy traps the H or He), contributing to the accumulation and different disposition depth of H and He in Mo.

1. Introduction

Because of high thermal conductivity and low sputtering erosion, Mo has been used in many current tokamaks (such as TRIAM-1M and FTU) and fusion studies [1–3]. Although Mo cannot be marked for plasma facing materials (PFMs) in ITER [4] as W due to neutron activation concerns, it still owns some superiority to W. For example, Mo is ductile at room temperature, with significantly lower brittle-ductile transition temperature, which makes it easier to be machined into shapes required for applications [5,6]. Mo also has better specific heat than W, making it easier to be thermally treated into structures with low thermal stresses [5]. Besides, H has higher diffusivity in Mo which leads to lower H retention [6–8]. Therefore Mo is still considered as an alternative for W [6,8,9]. The PFMs must be exposed to high heat and bombardment by H isotopes, He ions and high-energy neutrons escaping from plasma [10], which often precipitate into bubbles and therefore promote blister and induce embrittlement. Understanding H- and He-induced embrittlement of PFMs requires good knowledge of all basic processes affecting microstructural evolution, including dissolution and diffusion of solute light elements in the host. Concerning the interactions of H and He with materials, the early well-established essential qualitative insight is deduced from effective-medium theory (EMT) [11]. The detailed investigations of the behaviors of individual H and He in Mo are attainable owing to the advance in density functional theory (DFT) and computing power. Some DFT-calculations suggest that H (or He) is more energetically preferable to occupy tetrahedral interstitial site (TIS) rather than octahedral interstitial site (OIS) in perfect Mo [7,12–14]. H can diffuse easily from one TIS to the nearest TIS with a barrier of 0.16 eV [7]. However, the dissolution and diffusion of H and He in metals can be affected by the ubiquitously present and H and He irradiation-induced lattice vacancy. In other words, H and He atoms can diffuse quickly until they trapped by vacancy. Until now, tremendous efforts have been devoted to dealing with the

* Corresponding author. Tel.: +86 551 5591062.
E-mail address: csliu@issp.ac.cn (C.S. Liu).

0022-3115/$ - see front matter © 2012 Elsevier B.V. All rights reserved.
http://dx.doi.org/10.1016/j.jnucmat.2012.09.025

interplay of H and He with vacancy in metals. For example, the roles of vacancy on trapping H and He are emphasized in W [15–21] and α-Fe [22–24]; superabundant vacancy can be induced by H in Pd, Ni and Cr [25–28]; and the diffusion of H in Al [29] can be decreased due to the existence of vacancy. Since H and He coexist in PFMs, some experiments have been performed to investigate the interactions of H with He, especially the effect of He on retention and thermal release of deuterium [9,30]. Besides, some theoretical studies indicate that He-V complex can act as traps for foreign H atoms in W [20,21]. However, it is still a challenge, and the investigations of the behaviors of H and He in Mo are rare [7,12,31].

In this work, we will perform systemical first-principles calculations to investigate the interplays of a vacancy (or He-V complex) with H and He in Mo: the dissolution and diffusion properties of H and He in perfect system, nearby and inside a vacancy (or He-V complex). The site preference of H and He in Mo is analyzed by electronic density of state. The effects of single tetrahedral interstitial H and He on the nearby vacancy formation have been discussed. Besides, zero point energy corrections are considered for defect formation energies and diffusion barriers of H and He in Mo.

2. Computation method

Our calculations are performed within DFT as implemented in the VASP code with the projector augmented wave potential method [32]. The generalized gradient approximation and the Perdew–Wang functional are used to describe the electronic exchange and correlation effect [33]. The supercell composed of 128 Mo atoms ($4 \times 4 \times 4$) is used. The relaxations of atomic positions and optimizations of the shape and size of the supercell are performed. The plane wave cutoff and k-point density, obtained using the Monkhorst–Pack method [34], are both checked for convergence for the system to be within 0.001 eV per atom. Following a series of test calculations a plane wave cutoff of 500 eV is used and a k-point grid density of $3 \times 3 \times 3$ is employed. The structural optimization is truncated when the forces converge to less than 0.1 eV/nm. The defect formation energies are computed by the expression:

$$E_f = E_{nMo,mF} - nE_{Mo} - mE_F, \quad (1)$$

where F indicates foreign H or He, $E_{nMo,mF}$ is the total energy of the system with n Mo atoms and m foreign atoms like H or He, E_{Mo} is the energy per atom of pure crystal Mo and E_F is one half of the energy of H_2 molecule (−3.40 eV) and the energy of an isolated He atom (0.00 eV). In order to determine the migration barriers of H and He between different minima, the nudged elastic band (NEB) method is employed [35]. The vacancy formation energy with the presence of single H or single He atom at the nearest TIS is calculated by the formula:

$$E_V^f = E_{(n-1)Mo,F} - (E_{nMo,F} - E_{Mo}). \quad (2)$$

In the present work, the zero-point energy (ZPE) of H (or He) atom is calculated by summing up the normal modes of each H (or He) atom in the defect considered by the expression:

$$\mathrm{ZPE} = \frac{1}{2}\sum_i \hbar v_i, \quad (3)$$

where ħ and v_i are Plank's constant and the normal vibration frequencies, respectively. The vibration frequencies of H (or He) atom are calculated allowing harmonic vibrations only for H (or He) atom. The ZPE corrections on diffusion barriers of H (or He) are calculated by the difference in vibrational energies of saddle point and the ground state [36], that is, $\Delta E = \frac{1}{2}\sum_i \hbar v_i^S - \frac{1}{2}\sum_i \hbar v_i^G$, where v_i^S and v_i^G are the normal vibration frequencies of H (or He) at saddle point and ground state, respectively. The ZPE of $\frac{1}{2}H_2$ molecule is calculated to be 0.141 eV, which is in good agreement with other DFT-calculations [20,37–39]. Besides, ZPE of an isolated He atom is 0 eV.

3. Results and discussion

3.1. Individual hydrogen (or helium) atom in perfect molybdenum system

3.1.1. Formation of interstitial hydrogen (or helium)

Initially, we consider two kinds of high-symmetry interstitial sites for a single H (or He) atom in bcc Mo system: tetrahedral interstitial site (TIS) and octahedral interstitial site (OIS) shown in Fig. 1. The relative stability of the two sites is compared by computing the formation energies using Eq. (1). Our results with experimental and other theoretical values are displayed in Table 1. From Table 1, one can see that individual H and He atom prefer TIS over OIS by the respective energy of 0.26 eV and 0.17 eV, which is in good agreement with the other results without ZPE corrections [7,12]. When ZPE corrections are taken into account, the differences of H and He at TIS and OIS will be 0.17 eV and 0.12 eV, respectively. Therefore, ZPE corrections will narrow the energy difference of H (or He) at TIS and OIS, but will not change the order of the relative stability of H (or He) at TIS and OIS. The OIS has two closest Mo atoms located at 0.157 nm, and the TIS has four closest Mo atoms at 0.176 nm. We find that H at TIS and OIS pushes its nearest Mo away by 0.008 nm and 0.020 nm, respectively. While He at TIS and OIS pushes its closest Mo away by 0.010 nm and 0.026 nm, respectively. This may contribute to the relative stability of H and He in Mo. Due to the energy differences between the OIS and TIS for both H and He, only TIS is considered in further calculations.

3.1.2. Migration of interstitial hydrogen (or helium)

To investigate the diffusion behaviors of interstitial H and He in perfect Mo system, we compute the diffusion barriers of H and He atoms hopping from one interstitial site to another. Since having demonstrated that both H and He are more energetically favorable to occupy TIS, we concentrate on the diffusion of interstitial H and He between two TIS (Fig. 1): (a) from one TIS to the nearest TIS (TIS → TIS) and (b) from one TIS to the second nearest TIS, passing through an OIS (TIS → OIS → TIS). The energy barriers of H (or He) diffusion along the two paths are calculated and displayed in Table 2. We find that the energy barrier of the path TIS → TIS is significantly lower than that of the path TIS → OIS → TIS for both H

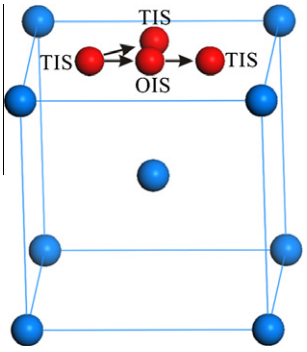

Fig. 1. The schematic view of the tetrahedral interstitial site (TIS) and octahedral interstitial site (OIS). The blue and red spheres indicate Mo atoms and the considered sites, respectively. The arrows indicate the diffusion paths. (For interpretation of the references to colour in this figure legend, the reader is referred to the web version of this article.)

Table 1
The calculated defect formation energies of H at TIS and OIS $E^f_{H\text{-}TIS}$ (eV) and $E^f_{H\text{-}OIS}$ (eV), and the defect formation energies of He at TIS and OIS $E^f_{He\text{-}TIS}$ (eV) and $E^f_{He\text{-}OIS}$ (eV). While defect formation energy with ZPE corrections are displayed in bracket.

	$E^f_{H\text{-}TIS}$	$E^f_{H\text{-}OIS}$	$E^f_{He\text{-}TIS}$	$E^f_{He\text{-}OIS}$
Other	0.62[a]	0.94[a]	5.28[b]	5.45[b]
Expt.	0.56[c]		4.97[d]	
This work	0.69(0.80)	0.95(0.97)	5.39(5.47)	5.56(5.59)

[a] Ref. [7].
[b] Ref. [12].
[c] Ref. [40].
[d] Ref. [41].

Table 2
The diffusion barriers of H and He in perfect Mo. The referenced data of H diffusion from one TIS to the closest TIS and from one TIS to the second neighboring TIS via an OIS are listed for comparison. ZPE corrections are considered for each barrier.

Reaction-path	Barrier (eV)		
	without ZPE	with ZPE	References
H			
TIS → TIS	0.16	0.12	0.16[a], 0.17[b], 0.23[c]
TIS → OIS → TIS	0.26	0.17	0.34[a]
He			
TIS → TIS	0.06	0.05	
TIS → OIS → TIS	0.17	0.12	

[a] Ref. [7].
[b] Ref. [40].
[c] Ref. [42].

and He. The ZPE corrections will lower the barriers of H and He diffusing along the two paths, but will not change the order of the preferred path. The calculated lowest-energy barrier for the path TIS → TIS of H is 0.16 eV, which is reduced to 0.12 eV when ZPE correction is considered. Compared with the experimental values of 0.17 eV [40] and 0.23 eV [42], our ZPE-corrected diffusion barrier of H in Mo is relatively lower, where the discrepancy may come from the ubiquitously present defects that slow down the diffusion of H in samples used in the experiments.

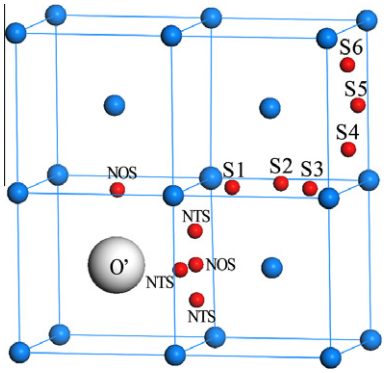

Fig. 2. The schematic view of all considered sites as labeled from S1 to S6 nearby a vacancy (or He-V complex) and O′, NTS and NOS inside a vacancy and He-V complex. O′ indicates the center of the vacancy, which can be occupied by He (i.e. He-V complex). The blue, red and white spheres indicate Mo atoms, considered sites and vacancy (or He-V complex) respectively. (For interpretation of the references to colour in this figure legend, the reader is referred to the web version of this article.)

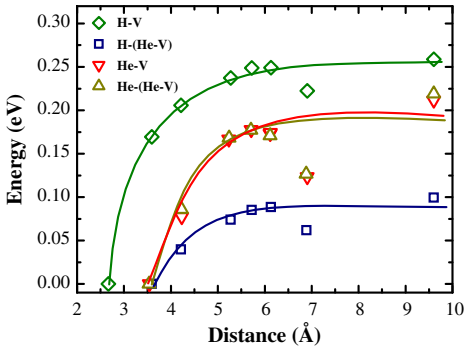

Fig. 3. The variation in the total energy in 128-site supercell with one vacancy (or He-V complex) and one interstitial H (or He) atom nearby the defect as a function of the distance between H (or He) and the center of the defect. The total energy is given relative to the energy of the system where H (or He) is placed at the stable site closest to the defect. The lines are guides to the eyes.

3.2. Individual hydrogen (or helium) atom nearby and inside a vacancy

3.2.1. Occupancy of interstitial hydrogen (or helium) nearby a vacancy

To investigate the influence of a vacancy on the occupancy properties of H and He in bcc Mo system, we firstly calculate vacancy formation energy using Eq. (1). The obtained vacancy formation energy of 2.91 eV is in good agreement with the experimental result of 2.9 eV [43] and other theoretical result of 2.61 eV [12]. Meanwhile, we also consider the effect of He-V complex on the behaviors of H and He. The site preference of interstitial H and He nearby a vacancy and He-V complex is investigated. And some TIS are taken into consideration: S1, S2, S3, S4, S5, and S6 (Fig. 2). The variations in the total energy of the system with one vacancy (or He-V complex) and one interstitial H (or He) atom as a function of the distance between H (or He) and the vacancy (or He-V complex) are displayed in Fig. 3. The total energy variation is given relative to the energy of the system where H (or He) is placed at the stable TIS nearest to the vacancy (or He-V complex): H at S1 nearby the vacancy, H at S2 nearby the He-V complex, and He at S2 nearby the vacancy and He-V complex. We note that H at S1 nearby the vacancy is locally stable, but H at S1 nearby He-V complex is unstable. Whereas He at S1 nearby the vacancy and He-V complex is unstable. In Fig. 3, one can see that both H and He are more energetically favorable to occupy TIS closer to the vacancy (or He-V complex). And the influence of the vacancy (or He-V complex) tends to disappear as H (or He) is displaced at more than 0.55 nm from the vacancy (or He-V complex). It is noted that ZPE corrections of the energy difference are relatively small, because the ZPE of H at all considered TIS keep ~0.253 eV and 0.319 eV nearby a respective vacancy and He-V complex, while He at all included TIS are ~0.087 eV and 0.158 eV nearby a vacancy and He-V complex, respectively. The relatively lower energy may enhance the concentration of H (or He) in the neighborhood of the vacancy (or He-V complex), which will be favorable for the accumulation of H and He in the vacancy (or He-V complex) and the growth of H, He as well as H–He mixed bubble. At the same time, we notice that the occupancy properties of interstitial He nearby the vacancy and He-V complex behave alike. Therefore we demonstrate that both H and He are more energetically preferable to the occupy the sites nearby a vacancy (or He-V complex) compared with the sites far away from the vacancy (or He-V complex).

3.2.2. Occupancy of hydrogen (or helium) inside a vacancy

The above results have clearly demonstrated that both H and He prefer to take the positions nearby a vacancy (or He-V complex) over that far from the defect. Next, we will investigate the occupancy properties of H and He inside a vacancy (or He-V complex). The calculated results with ZPE corrections display that single H atom at near octahedral site (NOS shown in Fig. 2) is most stable

with ~0.81 eV lower in formation energy than that of S1 nearby the vacancy. Unlike H, He prefers the geometric center of the vacancy (i.e. substitutional site (SS)) over S2 by ~3.53 eV. So the occupancy of H and He in Mo vacancy is alike to that in other metal vacancy [15,24,44]. The preference of H and He binding with the vacancy could be understood by two parts: one comes from smaller distortions caused by H (or He) at vacancy and the other contribution originates from chemical bonding. The results indicate that H at NOS and He at the center of vacancy pushes the closest Mo away by ~0.001 nm and 0.003 nm, respectively. Compared with the distortion induced by H and He at interstitial site, the distortions caused by H and He at vacancy are relatively smaller. Furthermore, in order to shed light on what underlies H and He site-preference at vacancy rather than the interstitial sites, we analyze the electronic structure of various H and He defects.

Similar to the discussion in W [45], we calculate site-projected electronic densities of states (DOS) for the TIS and NOS defects of H in Mo. And only the *d*-projected DOS of metal Mo atom closest to the H defect (Fig. 4a) and the *s*-projected DOS of the corresponding H itself (Fig. 4b) exhibit an interesting change. The *s*-projected DOS of H at NOS exhibits a broad induced states overlapping significantly with the *d*-projected DOS of Mo. The induced state shows a covalent bonding character via a strong hybridization of the *s*-projected DOS of H with the *d*-projected DOS of the closest Mo. However, the induced state of H atom at TIS is very local with a narrow distribution below the *d*-projected DOS of Mo, indicating less hybridization of the orbital with the closet Mo atom, while hybridization with transition metal is favorable for H. He is a closed-shell atom and any hybridization is energetically unfavorable for it. Seletskaia et al. discuss that the overall similarity in the shapes of the *d*-projected DOS of Fe and *p*-projected DOS of its neighbor He at TIS indicates hybridization between these states [46]. Moreover, the *p*-projected DOS of He at OIS is higher than that of He at TIS and both interstitial defects have higher DOS near the Fermi energy level than the DOS of He at SS in V, which agrees with the order of the site-preference of He, that is, SS, TIS, and OIS. Therefore, they also conclude that hybridizations of *p*-projected DOS of He and its neighbor metal atoms are responsible for the site-preference order of He [13]. In this work, as shown in Fig. 5a and c, it is noted that there is overall similarity in the shapes of the *d*-projected DOS of Mo atom and the *p*-projected DOS of its neighbor He atom at TIS, however, there is no similarity in the shape of *d*-projected DOS of Mo atom and the *p*-projected DOS of its neighbor He atom at SS. Besides, the *p* states of He at TIS is higher than that of He at SS near Fermi energy level, which indicates stronger hybridizes of He at TIS than at SS. Assuming that He is a completed spherically-symmetric *s* shell atom, acquiring *p*-projected DOS is unfavorable though He atom gets more *s*-projected DOS than the *p*-projected DOS. In this case, the larger the He *p*-projected DOS near the Fermi energy level, the less energetically favorable is the corresponding He defect configuration. The unfavorable He defect configuration leads directly to the larger formation energy of the He defect. This analysis agrees well with that by Seletskaia et al. [13,46].

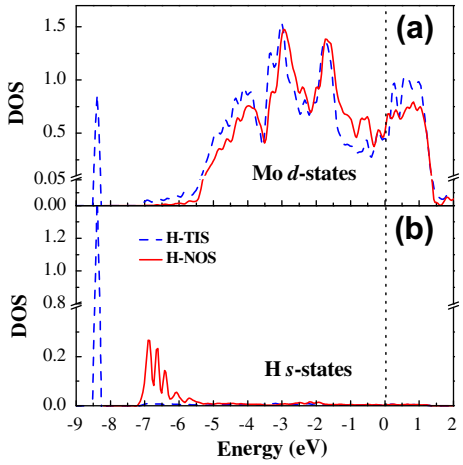

Fig. 4. (a) The *d*-projected DOS for Mo; (b) the *s*-projected DOS for H. The dashed and solid lines show the *d*-projected DOS of Mo with a H atom at respective TIS and NOS in the vacancy in (a), and the *s*-projected DOS of the H itself in (b).

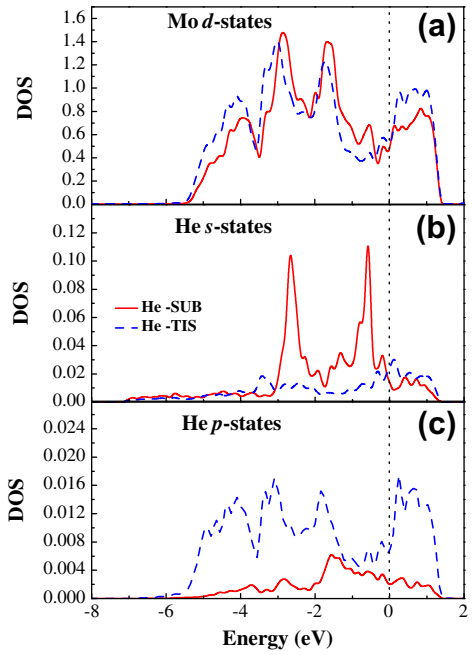

Fig. 5. (a) The *d*-projected DOS for Mo; (b) the *s*-projected DOS for He; (c) the *p*-projected DOS for He. In (a) the dashed and solid lines show the DOS of a Mo atom with a He atom at TIS and SS, respectively. In (b) and (c), the dashed and solid lines show the DOS of a He atom at TIS and SS.

We further investigate the occupancy of a single H (or He) atom at He-V complex. By testing many possible configurations, we find that both H and He are energetically preferable to stay at He-V complex rather than the sites nearby the defect. And the most favorable site for H at He-V complex is the near tetrahedral site (NTS) with the energy of ~0.015 eV lower than that of the near octahedral site (NOS) (Fig. 2). While He prefers the site, forming diatomic He–He dumbbell configuration along ⟨1 1 1⟩ direction with the already present He at He-V complex. The diatomic He–He is locally stable in three configurations at vacancy: dumbbell configurations along ⟨1 1 1⟩, ⟨1 1 0⟩, and ⟨1 0 0⟩ directions. We calculate

Table 3
The calculated formation energy of defects with diatomic H–H and He–He located in a single Mo vacancy, and the ZPE corrections are considered as comparisons. The distances of H–H and He–He are also listed.

Orientation	Distance (nm)	Formation energy (eV)	
		Without ZPE	With ZPE
He–He			
⟨1 0 0⟩	0.147	4.199	4.315
⟨1 1 0⟩	0.152	4.004	4.135
⟨1 1 1⟩	0.153	3.896	4.066
H–H			
⟨1 0 0⟩	0.248	1.658	1.596
⟨1 1 0⟩	0.219	1.713	1.744
⟨1 1 1⟩	0.191	2.581	2.487

the formation energy as well as the distance of He–He in the three configurations. As shown in Table 3, one can see that diatomic He–He prefers ⟨1 1 1⟩ dumbbell configuration rather than ⟨1 1 0⟩ dumbbell configuration by 0.11 eV and ⟨1 0 0⟩ dumbbell configuration by 0.30 eV. Meanwhile, it is notable that He–He dumbbell configurations along ⟨1 1 1⟩ direction corresponds to the longest He–He distance of 0.153 nm. As a comparison, we probe the formation energy of diatomic H–H in the three configurations similar to He–He. The calculated results displayed in Table 3 suggest that the ⟨1 0 0⟩ dumbbell configuration with the longest H–H distance of ~0.248 nm is the most stable. ZPE corrections slightly increase the formation energy of the three dumbbell configurations of diatomic He–He, and diatomic H–H along ⟨1 1 0⟩ direction. While the corrections reduce the formation energy of diatomic H–H long ⟨1 0 0⟩ and ⟨1 1 1⟩ directions. However, the relative stability of the three configurations of H–H (or He–He) is not changed. Therefore, one can see that the longest diatomic distance corresponds to the most stable configuration at vacancy for both H and He.

3.2.3. Migration of hydrogen (or helium) through a vacancy

In the above discussion, it has been found that TIS → TIS is the optimal diffusion path for both H and He with the barriers of 0.12 eV and 0.05 eV in perfect system, respectively. To probe the effect of vacancy (or He-V complex) on the migration behaviors of H and He, we investigate the energy landscape for H (or He) migration through the vacancy (or He-V complex). Our calculated energy profiles of H (or He) diffusion into and then out of the vacancy (or He-V complex) along the chosen paths are shown in Figs. 6–9. In all the figures, both the diffusion barriers of H (or He) with and without ZPE corrections are presented. The ZPE corrections generally reduce the diffusion barriers of H (or He), and we mainly discuss the barriers with ZPE corrections below. In Fig. 6, as a H atom approaches the vacancy, the diffusion barriers are reduced gradually from 0.109 eV (close to the lowest barrier in perfect system) to 0.006 eV, via the path from interstitial sites S5, S4, S3, S2, S1 to NOS. At the inside of the vacancy, H diffuses from one NOS to the closest NOS with the barrier of ~0.187 eV, which is much lower than the barrier of H diffusion out of the vacancy (~0.815 eV). However, once H jumps out of the vacancy, the barriers decrease from 0.265 eV to 0.118 eV as H diffuses from S1′ to S5′ via S2′, S3′ and S4′. So H can migrate easily into the vacancy but hardly jumps out of it. In this way H diffusion in Mo is seriously slowed down due to the existence of the vacancy, resulting in the accumulation of H in the vacancy. Therefore, it is understandable that the diffusion barriers of H in Mo observed in experiments are relatively larger than that we calculated. As a comparison, single H atom diffusion through a He-V complex is also considered. In Fig. 7, the diffusion barriers of H from S5 to NTS, via S4, S3, S2, and S1 reduce gradually as it approaches the complex like the behaviors of H diffusion to a vacancy. And the barrier of H diffusion from

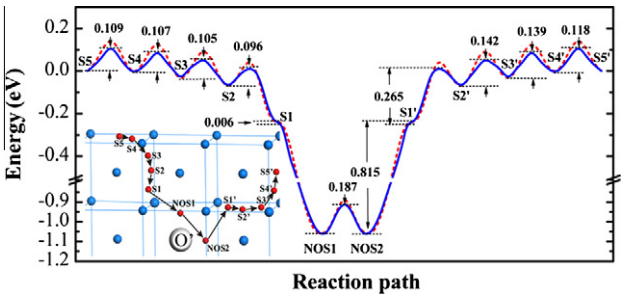

Fig. 6. The diffusion profile with the corresponding barriers of H from S5 to the inside of a vacancy, from NOS1 to NOS2 in the vacancy, and out of the vacancy from NOS2 to S5′, O′ indicates the center of the vacancy. The solid and dashed lines indicate the diffusion barriers with and without ZPE corrections.

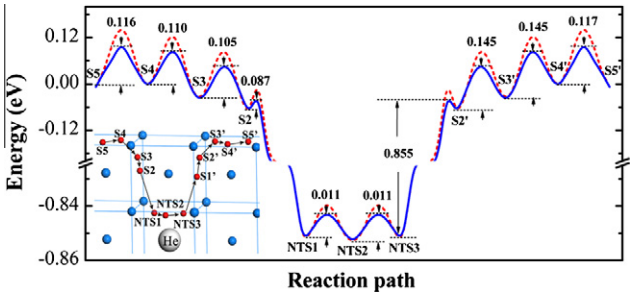

Fig. 7. The diffusion profile with the corresponding barriers of H from S6 to the inside of a He-V complex, from NTS1 to NTS3 via NTS2 in the complex, and out of the complex from NTS3 to S5′, He indicates a He atom occupying the center of the vacancy. The solid and dashed lines indicate the diffusion barriers with and without ZPE corrections.

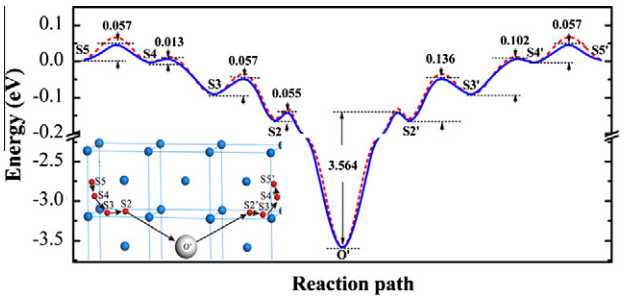

Fig. 8. The diffusion profile with the corresponding barriers of He from S5 to the center of a vacancy (O′) and then out of the vacancy from O′ to S5′. The solid and dashed lines indicate the diffusion barriers with and without ZPE corrections.

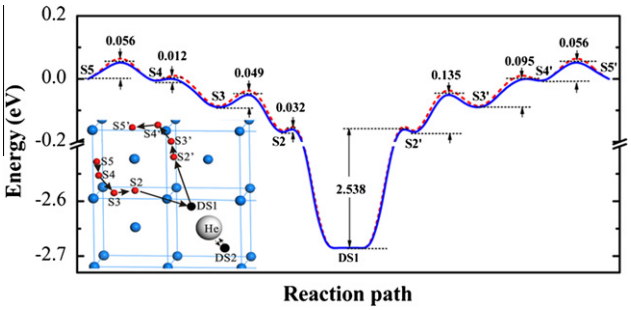

Fig. 9. The diffusion profile with the corresponding barriers of He from S5 to the site (DS1) to form ⟨1 1 1⟩ dumbbell configuration with the already present He (diffusion from vacancy center to DS2) in He-V complex and then out of the complex from DS1 to S5′, He indicates a He atom occupying the vacancy center. When a He atom migrates from S2 to DS1, He atom already presented in the vacancy center will diffuse to DS2 synergetically, and migrate back to the vacancy center from DS2 as the foreign He diffuses from DS1 to S2′. The solid and dashed lines indicate the diffusion barriers with and without ZPE corrections.

S1 to NTS even disappears, which is so-called 'downhill' drift diffusion. H could jump directly from S2 to He-V complex with the barrier of ~0.087 eV, which is still lower than the minimum diffusion barrier of H in perfect system. At the complex, H diffuses from one NTS to the closest NTS with the barrier of 0.011 eV. It is noted that the barrier of H diffusion out of the complex (~0.855 eV) is ~0.04 eV higher than that out of a vacancy. In other words, it is more favorable for H to accumulate at He-V complex than vacancy.

The migration of He from S5 to the center of a vacancy, passing through S4, S3 and S2 is investigated and displayed in Figs. 8. Unlike the gradual-decrease barriers of H approaching the vacancy, only the barriers of He diffusion from S4 to S3 is significantly reduced.

While He at S1 nearby the vacancy migrates into the vacancy in the style of 'downhill' drift diffusion. Because there is only one stable site for He at the vacancy, it moves directly from S2 to the center of the vacancy. However, He jumps out of the vacancy with the barrier of up to 3.564 eV, which is much higher than the barriers of H migration out of the vacancy and He-V complex. Clearly, a single Mo vacancy could strongly trap He atom, considerably slowing down the diffusion of He in Mo. So it is reasonable to conclude that the effect of vacancy on the accumulation of He is stronger than H. Besides, we also consider the effect of He-V complex on the diffusion of He. The barriers of He diffusion from S5 to S2 nearby a He-V complex is very similar to that of He diffusion nearby a vacancy, and He migrates directly from S2 to DS1, forming He–He dumbbell configuration along ⟨1 1 1⟩ direction with the already presented He at the He-V complex (Fig. 9). However, the jump-out barrier from the He-V complex is ~1.026 eV lower than that of He from a vacancy. So He located at He-V complex is relatively easier to jump out than at a vacancy. Meanwhile, when He migrates from S2 to DS1, the already presented He at the He-V complex center diffuses to DS2 synergetically, and it moves back to the center from DS2 as the foreign He diffuses from DS1 to S2′. To sum up, a vacancy and He-V complex could seriously slow down the migration of H and He in Mo, resulting in the accumulation of H and He in Mo, and the trapping ability of a vacancy is weaker than that of He-V complex on trapping H, but stronger than that of He-V complex on trapping He.

3.2.4. Effect of interstitial hydrogen (or helium) on nearby vacancy formation

Some experiments have qualitatively demonstrated that interstitial H in Pd can reduce vacancy formation energy: raising vacancy concentration in the metal [25–28]. Here we quantitatively calculate the vacancy formation energy with a H (or He) atom nearby. Having demonstrated that both H and He are more energetically favorable to occupy TIS in perfect system, we investigate the energetics of the Mo atoms closest to the H and He atoms. The calculated results with ZPE corrections display that the vacancy formation energies with the presence of single H and single He atom at TIS are reduced from 2.91 eV to 1.23 eV and −1.26 eV (Eq. (2)), respectively. Evidently, the vacancy formation with a He atom at TIS is much easier than that of H. Once a vacancy is produced the interstitial H or He atom will be caught by the vacancy. In other words, He atoms are caught by the already present and newly created vacancies, while more H atoms exist in the interstitial form. Combined with the diffusion of H in bulk and through a vacancy and He-V complex, we suggest that if metal Mo is exposed to H and He ions irradiation, it will also result in the extremely different disposition depth of the two light elements. And we believe that this may be the reason why He bubbles form right at ~10 nm to the W surface, while H bubbles are found at micrometers [47–49].

4. Conclusions

We have performed first-principles study of the occupancy and diffusion of H and He in perfect system, nearby a vacancy (or He-V complex), as well as inside a vacancy (or He-V complex) in Mo. In most of our results, zero point energy corrections taken into account. It is found that both H and He are more energetically preferable to occupy TIS over OIS in perfect system. While both H and He are more favorable to occupy the TIS nearby a vacancy (or He-V complex) rather than the TIS far away from the vacancy or complex. H and He at some TIS nearby a vacancy (or He-V complex) diffuse to the corresponding vacancy (or He-V complex) in the way of 'downhill' drift diffusion. H prefers to be situated at the sites near octahedral sites in a vacancy and the sites near tetrahedral sites in a He-vacancy complex. While He favors to take the geometric center in a vacancy and the site forming ⟨1 1 1⟩ dumbbell configuration with the already present He in a He-vacancy complex. Besides, it is found that the diffusion barriers of H and He into a vacancy (or He-V complex) are much smaller than that out of the vacancy (or He-V complex), slowing down the diffusion of H and He in Mo. At last, we find that He at TIS reduces the energy required for its nearby vacancy formation more considerably than that of H. The produced vacancy can trap H and He atom, which can contribute to the accumulation of H and He, and the different disposition depth of them in Mo.

Acknowledgements

This work was supported by the National Magnetic Confinement Fusion Program (Grant No.: 2011GB108004), the National Natural Science Foundation of China (Nos.: 91026002, 91126002) and the Strategic Priority Research Program of Chinese Academy of Sciences (Grant No.: XDA03010303), and by the Center for Computation Science, Hefei Institutes of Physical Sciences.

References

[1] S. Itoh, K.N. Sato, K. Nakamura, H. Zushi, M. Sakamoto, K. Hanada, E. Jotaki, K. Makino, S. Kawasaki, H. Nakashima, N. Yoshida, Nucl. Fusion 39 (1999) 1257.
[2] B. Angelini, S.V. Annibaldi, et al., Nucl. Fusion 45 (2005) S227.
[3] G.M. Wright, E. Alves, L.C. Alves, N.P. Barradas, P.A. Carvalho, R. Mateus, J. Rapp, Nucl. Fusion 50 (2010) 055004.
[4] ITER Physics Basis Editors, ITER Physics Expert Group Chairs and Co-Chairs, and ITER Joint Central Team and Physics Integration Unit, Nucl. Fusion 39 (1999) 2137.
[5] S.N. Nasser, W.G. Guo, M.Q. Liu, Scripta Mater. 40 (1999) 859.
[6] R.A. Causey, C.L. Kunz, D.F. Cowgill, J. Nucl. Mater. 337–339 (2005) 600.
[7] C. Duan, Y.L. Liu, H.B. Zhou, Y. Zhang, S. Jin, G.H. Lu, G.N. Luo, J. Nucl. Mater. 404 (2010) 109.
[8] S. Nagata, K. Takahiro, J. Nucl. Mater. 283–287 (2000) 1038.
[9] S. Nagata, K. Tokunaga, B. Tsuchiya, N. Ohtsu, T. Sugawara, T. Shikama, J. Alloy. Compd. 356–357 (2003) 326.
[10] J.B. Condon, T. Schober, J. Nucl. Mater. 207 (1993) 1.
[11] J.K. Nørskov, N.D. Lang, Phys. Rev. B 21 (1980) 2131.
[12] O. Runevall, N. Sandberg, J. Phys.: Condens. Matter 21 (2009) 335401.
[13] T. Seletskaia, Y. Osetsky, R.E. Stoller, G.M. Stocks, Phys. Rev. B 78 (2008) 134103.
[14] X.T. Zu, L. Yang, F. Gao, S.M. Peng, H.L. Heinisch, X.G. Long, R.J. Kurtz, Phys. Rev. B 80 (2009) 054104.
[15] Y.L. Liu, Y. Zhang, H.B. Zhou, G.H. Lu, F. Liu, G.N. Luo, Phys. Rev. B 79 (2009) 172103.
[16] K. Ohsawa, J. Goto, M. Yamakami, M. Yamaguchi, M. Yagi, Phys. Rev. B 82 (2010) 184117.
[17] K. Heinola, T. Ahlgren, K. Nordlund, J. Keinonen, Phys. Rev. B 82 (2010) 094102.
[18] C.S. Becquart, C. Domain, Nucl. Instrum. Methods B 255 (2007) 23.
[19] D. Kato, H. Iwakiri, K. Morishita, J. Nucl. Mater. 417 (2011) 1115.
[20] H.B. Zhou, Y.L. Liu, S. Jin, Y. Zhang, G.N. Luo, G.H. Lu, Nucl. Fusion 50 (2010) 115010.
[21] B. Jiang, F.R. Wan, W.T. Geng, Phys. Rev. B 81 (2010) 134112.
[22] P. Nordlander, J.K. Nørskov, F. Besenbacher, S.M. Myers, Phys. Rev. B 40 (1989) 1990.
[23] R. Nazarov, T. Hickel, J. Neugebauer, Phys. Rev. B 82 (2010) 224104.
[24] Y. Tateyama, T. Ohno, Phys. Rev. B 67 (2003) 174105.
[25] Y. Fukai, N. Ōkuma, Phys. Rev. Lett. 73 (1994) 1640.
[26] Y. Fukai, J. Alloy. Compd. 231 (1995) 35.
[27] Y. Fukai, Phys. Scripta T103 (2003) 11.
[28] Y. Fukai, The Metal-Hydrogen System: Basic Bulk Properties, Springer-Verlag, Berlin, 2005.
[29] H. Gunaydin, S.V. Barabash, K.N. Houk, V. Ozolins, Phys. Rev. Lett. 101 (2008) 075901.
[30] S.T. Picraux, J. Bøttiger, N. Rud, J. Nucl. Mater. 63 (1976) 110.
[31] K. Ohsawa, K. Eguchi, H. Watanabe, M. Yamaguchi, M. Yagi, Phys. Rev. B 85 (2012) 094102.
[32] G. Kresse, J. Furthmuller, Phys. Rev. B 54 (1996) 11169;
G. Kresse, J. Hafner, Phys. Rev. B 47 (1993) 558.
[33] J.P. Perdew, K. Burke, M. Ernzerhof, Phys. Rev. Lett. 77 (1996) 3865.
[34] H.J. Monkhorst, J.D. Pack, Phys. Rev. B 13 (1976) 5188.
[35] G. Mills, H. Jónsson, G.K. Schenter, Surf. Sci. 324 (1995) 305.
[36] K. Heinola, T. Ahlgren, J. Appl. Phys. 107 (2010) 113531.
[37] D.E. Jiang, E.A. Carter, Phys. Rev. B 70 (2004) 064102.
[38] W.A. Counts, C. Wolverton, R. Gibala, Acta Mater. 58 (2010) 4730.
[39] C. Wolverton, V. Ozolins, M. Asta, Phys. Rev. B 69 (2004) 144109.

[40] H. Katsuta, T. Iwai, H. Ohno, J. Nucl. Mater. 115 (1983) 206.
[41] L.M. Caspers, W. van Heugten, Deslft Progr. Rep. Ser. A: Chem. Phys., Chem. Phys. Eng. 1 (1974) 90.
[42] T. Tanabe, Y. Yamanishi, S. Imoto, J. Nucl. Mater. 191–194 (1992) 439.
[43] R. Ziegler, H.E. Schaefer, Mater. Sci. Forum 15 (1987) 145.
[44] G. Lu, E. Kaxiras, Phys. Rev. Lett. 94 (2005) 155501.
[45] D. Kato, H. Iwakiri, K. Morishita, J. Plasma Fusion Res. Ser. 8 (2009) 404.
[46] T. Seletskaia, Y. Osetsky, R.E. Stoller, G.M. Stocks, Phys. Rev. Lett. 94 (2008) 046403.
[47] R.J.K. Nicholson, J.M. Walls, J. Nucl. Mater. 76–77 (1978) 251.
[48] A.A. Haasz, M. Poon, J.W. Davis, J. Nucl. Mater. 266–269 (1999) 520.
[49] F.C. Sze, R.P. Doerner, S. Luckhardt, J. Nucl. Mater. 264 (1999) 89.